

FATIGUE-INDUCED CONCRETE FRACTURE UNDER COMBINED COMPRESSION AND SHEAR STUDIED USING STANDARD CYLINDER AND REFINED PUNCH-THROUGH SHEAR TEST SETUP

M. AGUILAR, A. BAKTHEER, H. BECKS, M. CLASSEN, R. CHUDOBA

RWTH Aachen University, Institute of Structural Concrete
Aachen, Germany
e-mail: maguilar@imb.rwth-aachen.de

Key words: concrete, fatigue, microplane model, thermodynamics, damage, plasticity

Abstract. To characterize the fatigue behavior of concrete, the standard cylinder test has been widely used for several decades. It is used as an essential test for investigating the uni-axial compressive fatigue behavior of concrete. However, the observed failure mechanism is primarily ascribed to the formation of shear bands during the later stages of fatigue life. This localized material zone exhibits an uncertain combination of shear and compressive stresses. An alternative test setup, referred to as refined punch-through shear test (PTST), has been introduced with the goal to enable an accurate control of a combined shear and compression fatigue loading. Initial experimental studies have shown that this setup leads to an enormous reduction in fatigue life scatter and an improvement in reproducibility due to a better control of the stress state in the localized zone. To analyze and interpret the experimental results, the microplane fatigue model MS1, recently introduced by the authors, is used. It aims to capture the fundamental inelastic mechanisms driving the tri-axial stress redistribution within a material zone during the fatigue damage process in concrete. Numerical studies are first presented to evaluate the stress profiles on a cylinder test before and after damage localization. Then, numerical simulations of PTST response under various levels of confinement can reproduce the monotonic and fatigue behavior of the tests. Finally, an analysis of the energy dissipation of the PTST is performed for cyclic loading under two different levels of confinement.

1 INTRODUCTION

The accurate prediction of fatigue life in concrete structures remains an unsolved issue that has garnered growing attention from the research community. There is an urgent need for a deeper understanding of concrete fatigue in order to tackle the environmental challenge ahead. This challenge involves striking a balance between the high carbon footprint associated with the concrete construction industry and the increasing global demand for concrete transportation and energy infrastructure. Consequently, future infrastructure must be constructed using less concrete while simultaneously extending

the service life of existing and future structures. Achieving such a transformative shift requires a comprehensive and rigorous depiction of fatigue phenomena, encompassing both the material and structural aspects.

In our recent work, we have proposed a dissipation hypothesis that attributes the main fatigue-induced degradation mechanism to a cumulative measure of inter-aggregate shear strain. This hypothesis leads to a new formulation of a pressure-sensitive interface model that can be embedded in both a discrete model of a material zone and a tensorial formulation of a microplane model. By making use of this hy-

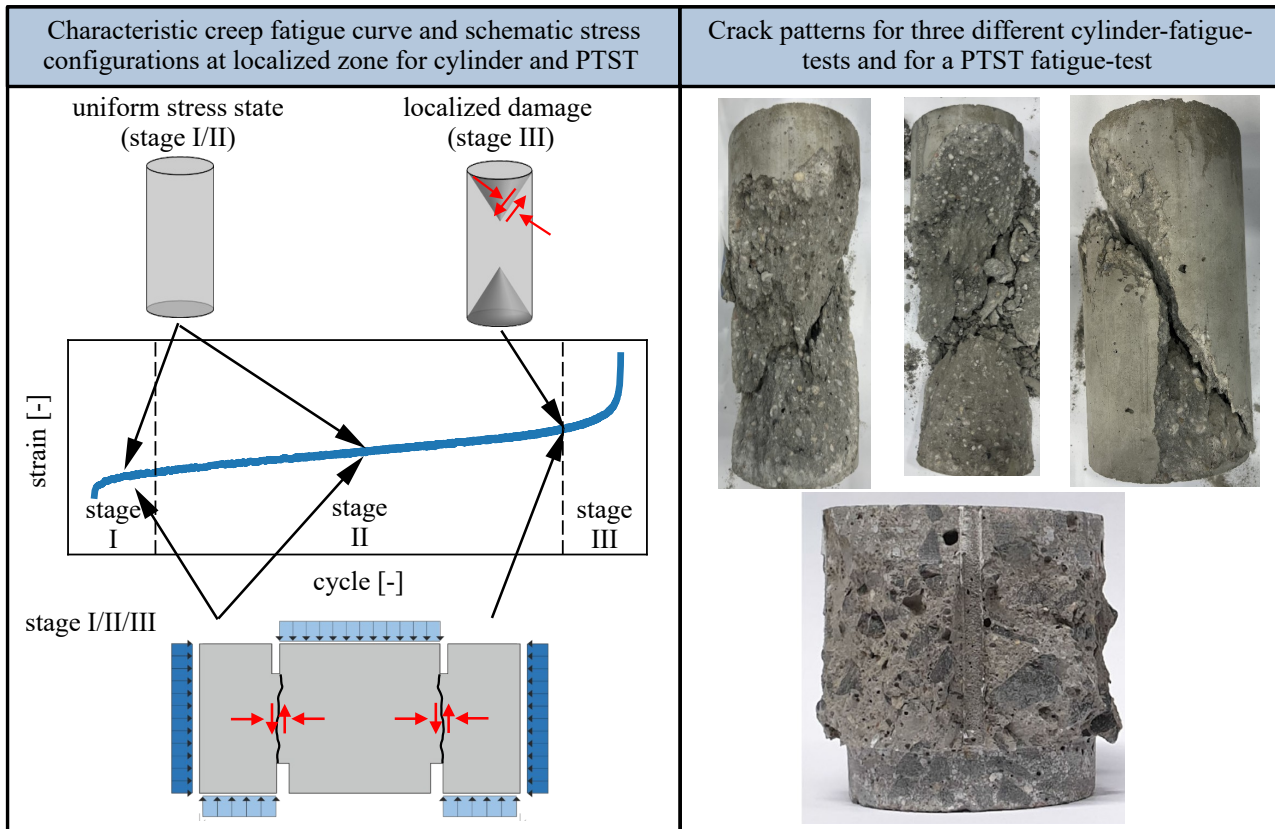


Figure 1: on the left: a typical creep fatigue curve of concrete with schematic characteristic fracture surface and stress configuration for cylinders and PTSTs. On the right: experimental fracture surfaces of three different cylinder tests and a PTST [8] after fatigue loading.

pothesis, the fatigue behavior of cementitious interfaces [1] and concrete under compressive fatigue loading [2] could be realistically modeled.

2 PUNCH-THROUGH SHEAR TEST

Luong et al. [3] originally introduced the cylindrical punch-through shear test (PTST) to investigate the material behavior of concrete and rock under combined shear and compression loading. Building upon this approach, Backers et al. [4] adopted a similar test to measure the fracture toughness of rock in mode II. In recent studies, the PTST has been employed to conduct preliminary investigations of concrete fatigue [5], which highlighted the significant influence of compressive stress on fatigue life under Mode II fatigue loading.

One of the main advantages of the PTST is the predetermined fracture surface, which ensures a consistent stress configuration in the lo-

calized zone during stages I, II, and III and across multiple tests, thus improving its reproducibility.

In contrast, in standard cylinder tests used to characterize the compressive fatigue behavior of concrete, the imposed uni-axial stress state can only be assumed during the stages I and II of the fatigue response. In stage III, the fatigue damage localizes into distinguished shear bands. The position and number of these shear bands depend on the friction between the load plates and the cylinder surfaces [6, 7] and can vary within a test series, as shown in Fig. 1. Once the specimen enters stage III, an a priori unknown state of combined compression and shear stress develops within the localized shear band, as numerically shown in Fig. 2. These numerical results correspond to the response of a cylinder subjected to a monotonic compressive load, in which the stress state before and after the localization is evaluated at the mid-

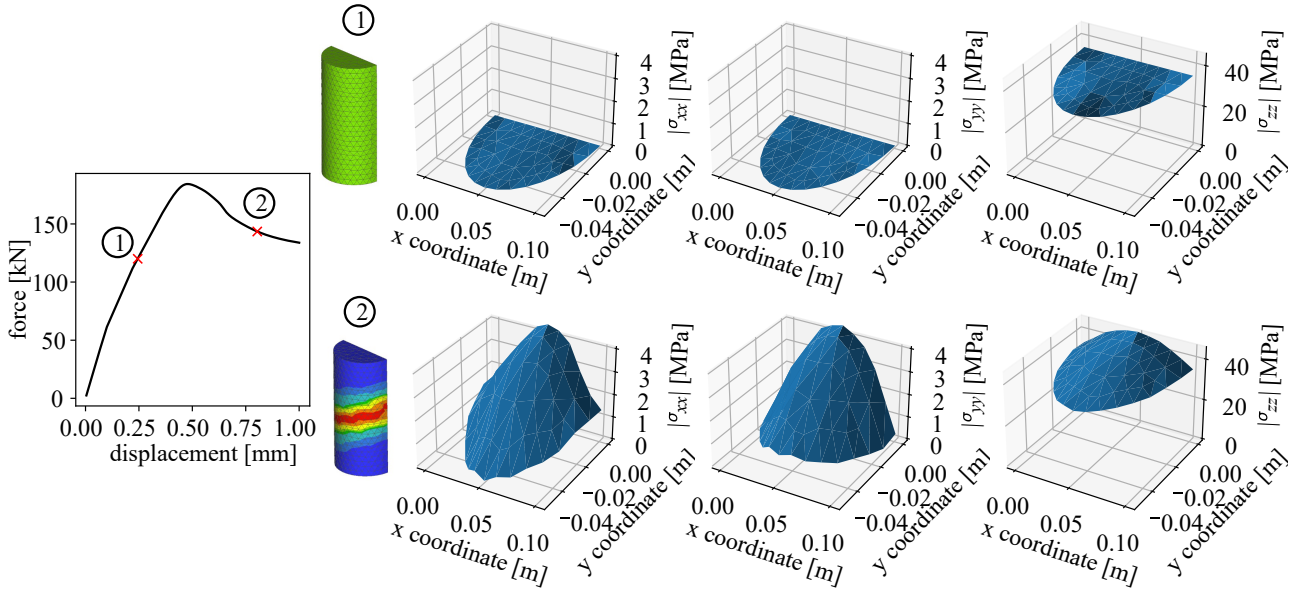


Figure 2: left: force-displacement curve for a monotonic compressive load on a cylinder ($h = 202$ mm, $d = 101$ mm) considering low friction on the top end and high friction on the bottom end between the loading plate and the specimen. The distributions of ε_I and σ_{ii} at points 1 and 2 of the simulation (before and after localization) are displayed in the top and bottom rows, respectively, right to the force-displacement curve.

plane of the cylinder. Before localization occurs, the stress state is uniform and uni-axial, as indicated by the uniform σ_{zz} component. However, once a shear band forms, typically during stage III of the fatigue life, the stress state becomes multi-axial and non-uniform. It is evident that the remaining fatigue life is significantly affected by the stress state present in the localized shear band of each individual test, potentially leading to a large scatter of the observed fatigue life, which typically spans between one and two orders of magnitude [2].

In order to validate the modeling fatigue hypothesis across various stress configurations, a test setup in which the applied normal and cyclic shear load can be adjusted independently within a tested material zone appears to be more suitable for investigating the fatigue response in a wider range of stress configurations than the standard cylinder tests. However, there is currently no standardized test that effectively characterizes the fatigue shear behavior of confined concrete. In response to this gap, the authors have recently proposed a novel version of the PTST to specifically address this challenge [5, 8]. This refined PTST setup, which

allows the simultaneous and independent application of shear and compressive loading, can be used to systematically isolate the influence of the degree of confinement on the fatigue life of high-strength concrete under subcritical fatigue shear loading [8]. The use of this new test setup has significantly reduced the scatter in the measured fatigue life by providing better control of the stress state in the localized zone. In contrast to the standard cylinder test, a predetermined failure surface could be achieved for all the tested specimens, as shown in Fig. 1. Due to the reduction in the scatter of the tested fatigue life, it becomes feasible to investigate the load sequence effect, which is crucial for the accurate estimation of the fatigue life of concrete structures.

3 MICROPLANE FATIGUE MODEL

To analyze and interpret the experimental results of the PTST reported in [5, 8], we employ the recently developed material model MS1 [2, 10]. This model introduces the cumulative shear fatigue hypothesis at the microplane level. By linking the fatigue process to a cumulative measure of inelastic shear

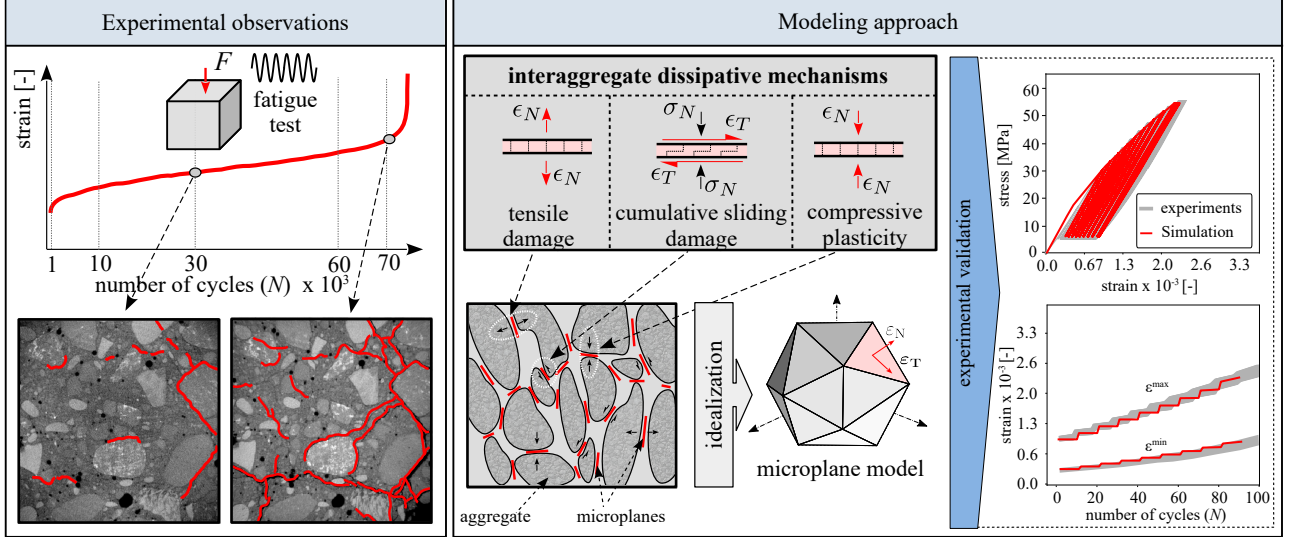


Figure 3: left: experimental observations of microcrack development under compressive fatigue loading using X-ray micro-CT images obtained by Skarzynski et al. [11]. Center: schematic interaggregate dissipative mechanisms included in MS1 and illustration of the microstructure containing a system of dissipative microplanes. Right: schematic experimental validation procedure presented in [2].

strain, it becomes possible to reproduce the tri-axial stress redistribution occurring within the material structure when subjected to pulsating subcritical loading. This fatigue-induced stress redistribution aligns with the observed degradation process documented by Skarzynski et al. [11], which suggests that crack initiation and propagation during fatigue loading predominantly take place along interfaces between the hardened cement paste and aggregates, as shown in Fig. 3. The model, formulated within the microplane framework, utilizes the kinematic constraint to project the macroscopic strain tensor onto the microplanes and applies the principle of virtual work and energy equivalence to homogenize the microplane stresses, secant, and plastic strain tensors.

3.1 Thermodynamically based formulation

At the level of the idealized microplane, which represents the inter-aggregate behavior within a 3D material structure in a specific direction, thermodynamically based constitutive laws are introduced to capture the degradation mechanisms. The macroscopic Helmholtz free energy is then formulated as the integral of the sum of the microplane normal and tangential

thermodynamic potentials.

$$\begin{aligned} \psi^{\text{mac}} &= \frac{3}{2\pi} \int_{\Omega} \psi^{\text{mic}} d\Omega = \\ &= \frac{3}{2\pi} \int_{\Omega} \psi_N d\Omega + \frac{3}{2\pi} \int_{\Omega} \psi_T d\Omega. \end{aligned} \quad (1)$$

By projecting the thermodynamic potentials onto the normal and tangential directions, it becomes possible to distinguish and account for the specific dissipative mechanisms that occur in each direction, schematically depicted in Fig. 3.

Normal direction: the microplane thermodynamic potential corresponding to the normal direction is defined as follows:

$$\begin{aligned} \rho \psi_N^{\text{mic}} &= \frac{1}{2} [1 - H(\sigma_N) \omega_N] E_N (\epsilon_N - \epsilon_N^p)^2 \\ &+ \frac{1}{2} K_N z_N^2 + \frac{1}{2} \gamma_N \alpha_N^2, \end{aligned} \quad (2)$$

where ρ represents the material density, E_N is the normal elastic stiffness defined as $E/(1 - 2\nu)$, where E represents the elastic modulus and ν denotes the Poisson's ratio. The Heaviside function $H(\sigma_N)$ allows for the distinction between tension and compression in the normal behavior.

When the microplane experiences compression in the normal direction, the Heaviside function can be expressed as $H(\sigma_N < 0) = 0$. In this case, the microplane only exhibits plastic deformation, and the normal damage remains unchanged.

When the microplane is subjected to tension in the normal direction, the Heaviside function takes the value $H(\sigma_N > 0) = 1$. In this situation, the microplane is activated for damage evolution. Under tension the normal plastic deformation does not change. The isotropic and kinematic hardening moduli are denoted as K_N and γ_N , respectively. Additionally, the thermodynamic internal variables encompass the plastic normal strain ε_N^p , the normal damage ω_N , as well as the isotropic and kinematic hardening variables z_N and α_N , respectively. To determine the conjugate thermodynamic forces, the thermodynamic potential (Eq. (2)) is differentiated with respect to each internal variable.

Tangential direction: The primary cause of fatigue damage leading to material deterioration at pulsating subcritical stress levels is considered to be the cumulative sliding in the tangential direction. To incorporate this mechanism, the tangential constitutive behavior of a microplane is introduced, following a similar approach to the pressure-sensitive interface model presented in [14]. In this model, fatigue damage is associated with the cumulative inelastic slip.

Analogously, the Helmholtz free energy function of a microplane in the tangential direction is expressed as follows:

$$\begin{aligned} \rho\psi_T^{\text{mic}} = & \frac{1}{2}(1 - \omega_T)E_T(\boldsymbol{\varepsilon}_T - \boldsymbol{\varepsilon}_T^\pi) \cdot (\boldsymbol{\varepsilon}_T - \boldsymbol{\varepsilon}_T^\pi) \\ & + \frac{1}{2}K_T z_T^2 + \frac{1}{2}\gamma_T \boldsymbol{\alpha}_T \cdot \boldsymbol{\alpha}_T, \end{aligned} \quad (3)$$

where the tangential elastic stiffness is denoted as $E_T = E(1 - 4\nu)/((1 + \nu)(1 - 2\nu))$. Additionally, K_T and γ_T represent the isotropic and kinematic strain hardening moduli, respectively. The thermodynamic internal variables consist of the inelastic tangential strain vector $\boldsymbol{\varepsilon}_T^\pi$, the damage tangential variable ω_T , the

isotropic hardening variable z_T , and the kinematic hardening vector $\boldsymbol{\alpha}_T$.

Similar to the normal direction, the conjugate thermodynamic forces are obtained by differentiating the thermodynamic potential (3) with respect to each state variable. For a comprehensive description of the model, including the governing threshold functions and evolution laws, see [2].

3.2 Evaluation of energy dissipation

The evaluation of energy dissipation for an isothermal process under the assumption of small strains is expressed using the Clausius-Duhem inequality. Specifically, for the normal direction, it can be given as follows:

$$\dot{\mathcal{D}}_{\text{int}}^N = -\rho\dot{\psi}_N + \sigma_N\dot{\varepsilon}_N \geq 0, \quad (4)$$

by replacing $\dot{\psi}_N$, utilizing the chain rule, operating as described in [12, 13], and integrating the dissipation rates with respect to the pseudo time t , the resulting expression yields the total energy dissipation associated with a microplane in the normal direction:

$$\begin{aligned} \mathcal{D}_{\text{int}}^N = & \int_0^t [\sigma_N\dot{\varepsilon}_N^p - Z_N\dot{z}_N \\ & - X_N\dot{\alpha}_N + Y_N\dot{\omega}_N] dt. \geq 0. \end{aligned} \quad (5)$$

The energy dissipation for the tangential direction is evaluated in a similar manner to the normal direction. Starting with the Clausius-Duhem inequality, which can be expressed as follows:

$$\dot{\mathcal{D}}_{\text{int}}^T = -\rho\dot{\psi}_T + \boldsymbol{\sigma}_T\dot{\boldsymbol{\varepsilon}}_T \geq 0. \quad (6)$$

Following the same procedure as in the case of the normal direction, the total energy dissipation can be represented as:

$$\begin{aligned} \mathcal{D}_{\text{int}}^T = & \int_0^t [\boldsymbol{\sigma}_T \cdot \dot{\boldsymbol{\varepsilon}}_T^\pi - Z_T\dot{z}_T \\ & - \mathbf{X}_T \cdot \dot{\boldsymbol{\alpha}}_T + Y_T\dot{\omega}_T] dt \geq 0. \end{aligned} \quad (7)$$

By integrating the contributions of each microplane for both normal and tangential directions, the macroscopic energy dissipation is

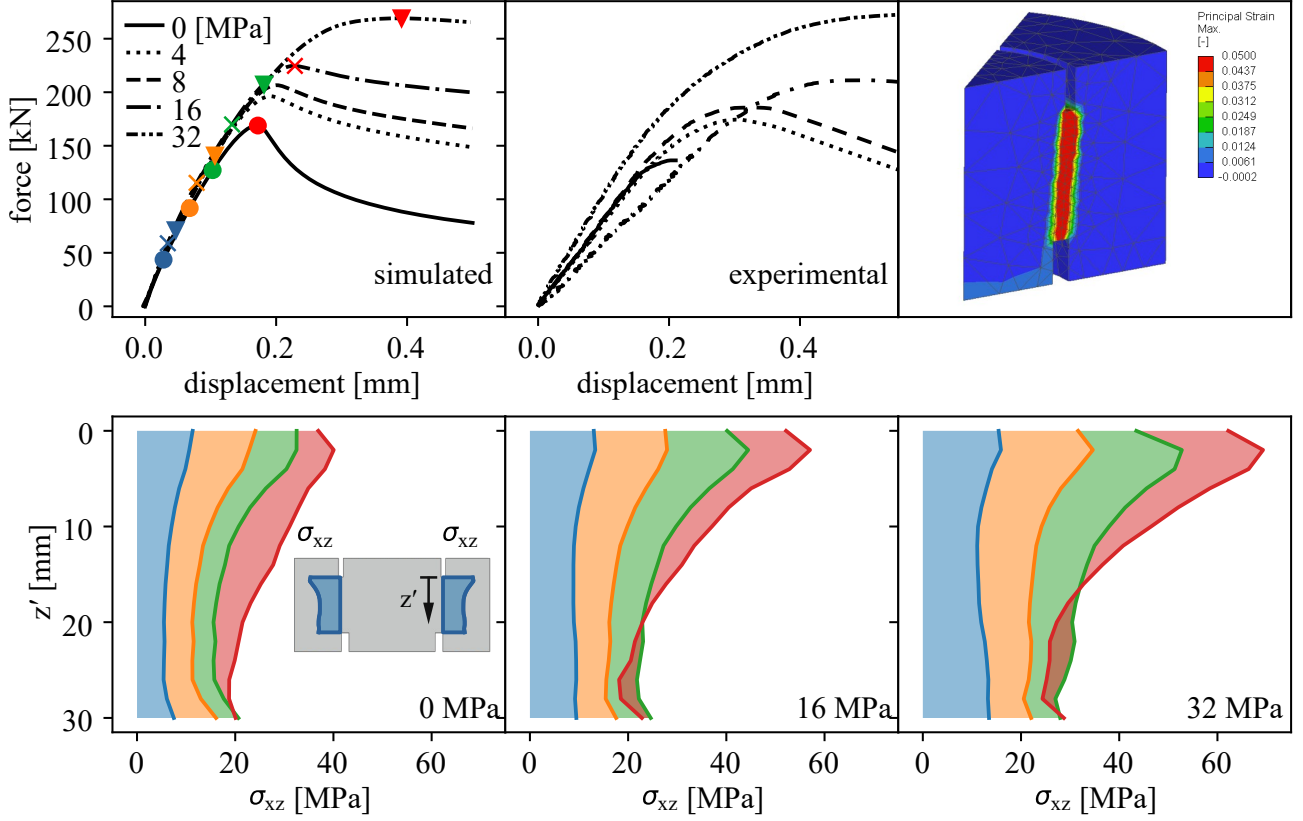


Figure 4: Top left and middle figures correspond to the simulated and experimental [8] monotonic behavior for the PTST, respectively. Top left panel displays the failure surface for experimental and simulated results. The bottom row shows the shear stress distribution σ_{xz} along the ligament height for 25 (blue), 50 (orange), 75 (green), 100 % (red) for the indicated confinement level. Material parameters: $E = 39226$, $\nu = 0.18$, $\epsilon_N^0 = 1e^{-5}$, $A_d = 7000$, $\sigma_N^0 = 40.0$, $\gamma_N = 80000$, $K_N = 14000$, $\sigma_T^0 = 10.0$, $\gamma_T = 120000$, $K_T = 1200$, $S_T = 0.01$, $r_T = 8.5$, $c_T = 7.5$, $p_T = 7.5$, $m_T = 0.05$

evaluated as:

$$\begin{aligned} \mathcal{D}_{\text{int}}^{\text{mac}} &= \frac{3}{2\pi} \int_{\Omega} \mathcal{D}_{\text{int}}^{\text{mic}} d\Omega \\ &= \frac{3}{2\pi} \int_{\Omega} \mathcal{D}_{\text{int}}^{\text{N}} d\Omega + \frac{3}{2\pi} \int_{\Omega} \mathcal{D}_{\text{int}}^{\text{T}} d\Omega. \end{aligned} \quad (8)$$

4 NUMERICAL RESULTS

4.1 Monotonic behavior

To assess the capability of the microplane material model MS1 to reproduce the behavior of the PTST under varying levels of normal confinement, Fig. 4 displays a study conducted using Mode II displacement control loading at both numerical and experimental results. The model parameters were calibrated to reproduce the monotonic experimental strength of the material. In particular, five levels of confinement were considered, which are 0, 4, 8, 16, and 32 MPa.

The numerically obtained force-displacement curves for the five studied cases are illustrated in Fig. 4 top left panel. As apparent, there is an increase in both the peak load and, to a slight extent, in the stiffness for a growing level of confinement. The corresponding experimental monotonic behavior is shown in Fig. 4 top middle panel. There is good agreement between the numerical and experimental peak loads for each confinement level.

At the top right in Fig. 4 the numerical model discretization and its associated fracture surface in terms of ϵ_I is displayed. The bottom row shows the shear stress profile along the ligament of the PTST, where the shear stress σ_{xz} is averaged over the ligament thickness and plotted over the height. To that end, a local coordinate system is introduced as schematically depicted at the bottom left panel. Shear stresses are eval-

uated for confinement levels of 0, 16, and 32 MPa at four points on the respective load displacement curves, corresponding to 25 (blue), 50 (orange), 75 (green), and 100 % (red) of the associated peak load. The observed patterns indicate that the shear stress profiles are relatively constant for the case corresponding to 25% of the maximum peak load. However, as the load levels increase, the shear stress in the upper region of the ligament experiences an upward trend, particularly for higher confinement levels. This phenomenon can be attributed to the combination of two effects acting in the radial direction. Firstly, there is the influence of an increased quasi-uniform confinement, and secondly, there is the bending effect caused by the applied vertical load. These effects result in a higher compression of the upper part of the ligament, where the higher confinement level is combined with the increased compressive stresses due to the bending action of the higher peak load. Consequently, there is a significant increase in shear strength in the upper region of the ligament, which can be attributed to the pressure sensitivity of the material formulation. In contrast, the lower part of the ligament experiences a partial offsetting effect, as the higher degree of confinement is counteracted by higher superimposed tensile stress resulting from the bending action of the increased peak load.

Although the shear stress profiles are not uniform, it is important to point out that the key advantage of the test setup is the ability to control the lateral and vertical loading as well as the fracture surface. The resulting stress profile is solely dependent on the applied loads and the specimen geometry and thus possible to numerically determine. This stands in contrast to the cylinder test, where the failure surface can vary across different tests, resulting in varying stress configurations being tested.

4.2 Fatigue behavior

To examine the ability of the model to reproduce the response of confined concrete under cyclic subcritical shear loading, a load scenario with a subcritical step-wise increasing up-

per load level has been used. The cyclic loading consisted of 10 cycles applied at each load level, starting with a maximum shear load of $S_{\max} = 0.5$ and incrementally increasing it by $\Delta S_{\max} = 0.05$. Meanwhile, the lower load level remained constant at $S_{\min} = 0.05$. This loading scenario offers the possibility to rapidly and effectively characterize the subcritical behavior of concrete for various loading amplitudes.

In the top left of Fig. 5, the simulated prediction of the force-displacement response under the loading scenario described above is shown for confinement levels of 15 and 30 MPa. This prediction is made using the material parameters obtained from the previous monotonic study shown in Fig. 4, calibrated using the first test series from [8]. Unfortunately, a corresponding cyclic loading scenario was not applied to the same batch of specimens, so a quantitative comparison of the prediction with a measured response is not possible. Still, to provide a qualitative comparison, we show the results for this loading scenario obtained for the second test series presented in the paper [8]. These specimens achieved higher peak load values, as indicated by the dashed lines.

The current calibration also allows for qualitative analysis of the stress distribution at the ligament for different loading amplitudes, as shown in Fig. 5, top right panel. The shear stress profiles are obtained and presented analogously to Fig. 4 for the confinement level of 30 MPa for 50, 60, 70, 80, 90 and 95% of the maximum peak load. The breakdown of energy dissipation is shown in the bottom row, with the left and middle figures corresponding to the cumulative energy dissipation associated with each dissipative mechanism along the cycles for the case of 15 and 30 MPa confinement levels, respectively. The lower right figure shows the accumulated energy dissipation for each confinement level due to damage and plasticity, without distinguishing between normal and tangential directions. It can be observed that there is a clear increment of the plastic energy dissipation, while the damage energy dissi-

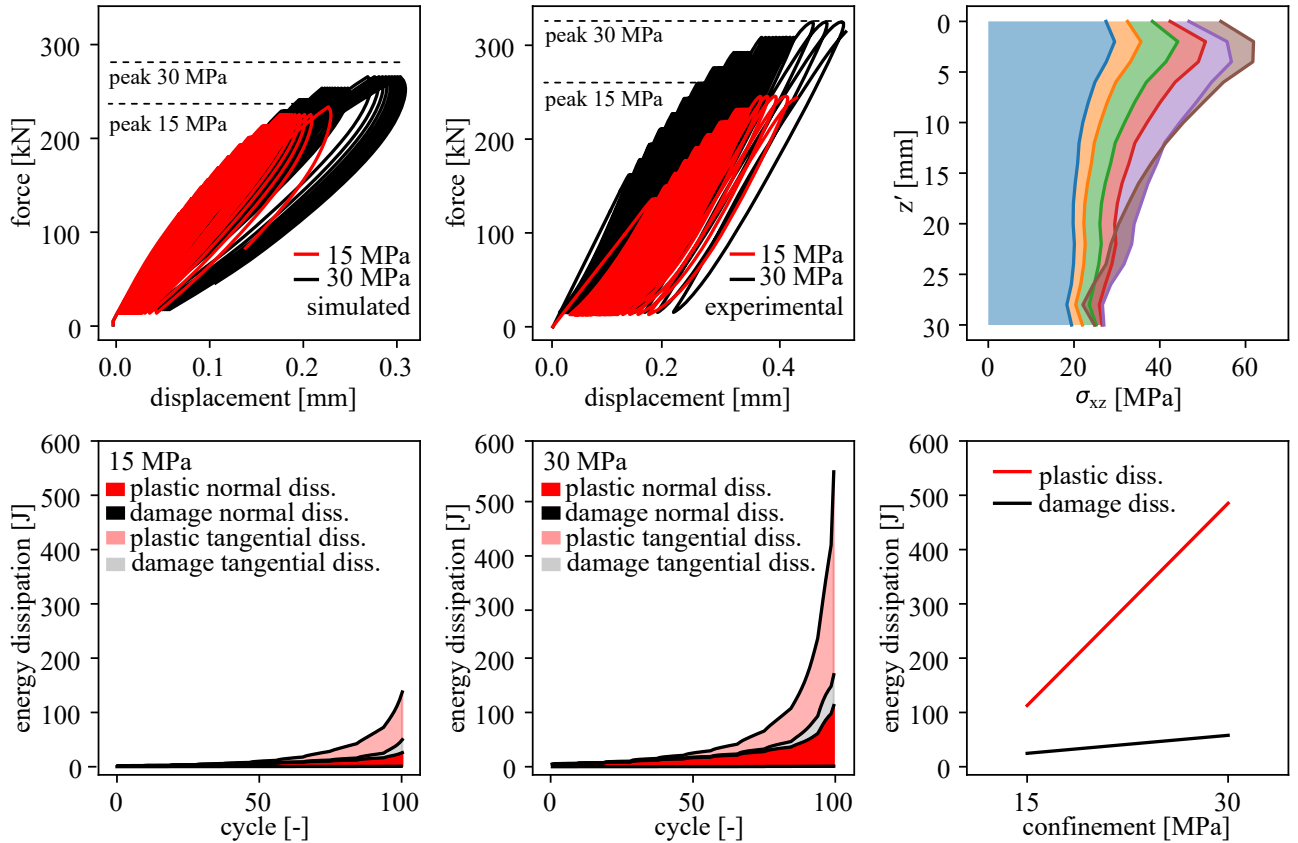


Figure 5: Top left and middle figures correspond to the simulated and experimental [8] step-wise increasing cyclic behavior for the PTST, respectively. Top left panel displays the shear stress distribution σ_{xz} along the ligament height for 50 (blue), 60 (orange), 70 (green), 80 (red), 90 (purple) and 95 % (brown) for a confinement level of 30 MPa. Bottom left and middle figures corresponds to the cumulative energy dissipation associated with each dissipative mechanism along the cycles for the case of 15 and 30 MPa confinement levels, respectively. Lower right figure shows the accumulated energy dissipation for each confinement level due to damage and plasticity. Material parameters as specified in the caption of Fig. 4

pation remains in comparison of the same order. Numerical studies previously presented by the authors in [12, 13] consistently yield similar results, where the energy dissipation attributed to damage does not change as dramatically as the plastic energy dissipation for simulations of the same test setup under the same boundary conditions.

5 CONCLUSIONS

To characterize the fatigue behavior of confined concrete subjected to shear fatigue loading, a newly developed version of the PTST has been used. The novel test setup allows independent control of the confinement level and shear loading, as well as the predetermination of the fracture surface. In contrast, the standard cylin-

der test aims to induce a uniform and uni-axial compression stress in the specimen. However, macroscopically uniform stress profile can only be assumed during the initial stages of fatigue life corresponding to the stage I and II in the fatigue creep curve. In stage III, when the damage localizes into a shear band, a non-uniform and undefined combination of compressive and shear stress configuration occurs. The stress state in the localized zone depends on factors such as the position, inclination, and number of macro cracks, which in turn is influenced by the friction between the cylinder and loading plate.

The PTST offers the possibility to study and characterize the fatigue behavior of concrete under combined compressive and shear loading in a systematic manner. Experimen-

tal results covering the confined monotonic and subcritical cyclic shear behavior of concrete are presented and qualitatively reproduced using the MS1 model in combination with a finite element (FE) model. The pressure-sensitive formulation employed in MS1 at the microplane level enables the reproduction of increased shear strength with increasing confinement, thereby reproducing the experimentally observed increase of the peak load with higher levels of confinement.

Regarding the fatigue behavior, the model MS1 captures the propagation of damage in concrete under subcritical pulsating loading, with an accelerated damage process observed when the loading amplitude is increased, qualitatively complying with the Wöhler (S-N) curve of concrete. Furthermore, by utilizing the thermodynamic formulation of the MS1 microplane model, it becomes possible to evaluate the energy dissipation attributed to each considered dissipative mechanism. These studies reveal significant variations in plastic energy dissipation depending on the specific loading scenario, while damage dissipation remains relatively constant across various loading scenarios. These insights provide a foundation for more realistic predictions of fatigue life in concrete structures.

ACKNOWLEDGMENTS

The authors gratefully acknowledge the support for this research by the German Research Foundation (Deutsche Forschungsgemeinschaft DFG), in (I) the scope of the Priority Program SPP2020 "Cyclic deterioration of high-performance concrete in an experimental virtual lab", (Project number: 441550460), (II) the scope of the joint project "Energy dissipation-based approach to stochastic fatigue of concrete considering interacting time and temperature effects", Project number: 471796896).

REFERENCES

[1] Chudoba, R., Vořechovský, M., Aguilar, M., and Baktheer, A. 2022. Coupled sliding–decohesion–compression model

for a consistent description of monotonic and fatigue behavior of material interfaces. *Computer Methods in Applied Mechanics and Engineering* **398**:115259. doi:/10.1016/j.cma.2022.115259

- [2] Baktheer, A., Aguilar, M. and Chudoba, R. 2021. Microplane fatigue model MS1 for plain concrete under compression with damage evolution driven by cumulative inelastic shear strain. *International Journal of Plasticity* **143**:102950. doi: 10.1016/j.ijplas.2021.102950
- [3] Luong, M.P. 1989. Fracture behaviour of concrete and rock under mode II and mode III shear loading. *Fracture of Concrete and Rock: Recent Developments* 18-26.
- [4] Backers, T., Stephansson, O., and Rybacki, E. 2002. Rock fracture toughness testing in Mode II—punch-through shear test. *International Journal of Rock Mechanics and Mining Sciences* (2002) **39.6**:755-769. doi: 10.1016/S1365-1609(02)00066-7
- [5] Becks, H. and Classen, M. 2021. Mode II behavior of high-strength concrete under monotonic, cyclic and fatigue loading. *Materials* **14.24**:7675. doi: 10.3390/ma14247675
- [6] Cusatis, G., Mencarelli, A., Pelessone, D., Baylot, J. 2011. Lattice Discrete Particle Model (LDPM) for failure behavior of concrete. II: Calibration and validation. *Cement and Concrete Composites* **33.9**:891-905. doi: 10.1016/j.cemconcomp.2011.02.010
- [7] Středulová, M., Lisztwan, D., Eliáš, J. 2022. Friction effects in uniaxial compression of concrete cylinders. *Procedia Structural Integrity* **42**:1537-1544. doi: 10.1016/j.prostr.2022.12.194
- [8] Becks H., Aguilar M., Chudoba R., Classen M. 2022. Characterization of high-strength concrete under monotonic

- and fatigue mode II loading with actively controlled level of lateral compression. *Materials and Structures* **55**:252. doi: [10.1617/s11527-022-02087-4](https://doi.org/10.1617/s11527-022-02087-4)
- [9] Aguilar, M., Becks, H., Baktheer, A., Classen, M., and Chudoba, R. (2022). Effect of lateral confinement on concrete fatigue life under shear loading. *In Computational Modelling of Concrete and Concrete Structures, Euro-C 2022*. doi: [10.1201/9781003316404-19](https://doi.org/10.1201/9781003316404-19)
- [10] Baktheer, A., Aguilar, M., Hegger, J., and Chudoba, R. 2019. Microplane damage plastic model for plain concrete subjected to compressive fatigue loading. *FraMCoS-X*. doi: [10.21012/FC10.233196](https://doi.org/10.21012/FC10.233196)
- [11] Skarzynski, L., Marzec, I. and Tejchman, J. 2019. Fracture evolution in concrete compressive fatigue experiments based on X-ray micro-CT images. *International Journal of Fatigue*. **122**:241–252. doi: [10.1016/j.ijfatigue.2019.02.002](https://doi.org/10.1016/j.ijfatigue.2019.02.002)
- [12] Aguilar, M., Baktheer, A., and Chudoba, R. 2021. Numerical investigation of load sequence effect and energy dissipation in concrete due to compressive fatigue loading using the new microplane fatigue model MS1. *COMPLAS*, Onate, E., Peric, D., Chiumenti, M., de Souza Neto, E., Eds. doi: [10.23967/complas.2021.053](https://doi.org/10.23967/complas.2021.053)
- [13] Aguilar, M., Baktheer, A. and Chudoba, R. 2023, On the energy dissipation in confined concrete subjected to shear cyclic loading. *PAMM* 22: e202200301. doi: [10.1002/pamm.202200301](https://doi.org/10.1002/pamm.202200301)
- [14] Baktheer, A., and Chudoba, R. 2018. Pressure-sensitive bond fatigue model with damage evolution driven by cumulative slip: Thermodynamic formulation and applications to steel-and FRP-concrete bond. *International Journal of Fatigue* **113**:277-289. doi: [10.1016/j.ijfatigue.2018.04.020](https://doi.org/10.1016/j.ijfatigue.2018.04.020)